SEARCHING FOR GRAPHITE NODULE NUCLEI USING AUTOMATED SEM/EDX ANALYSIS

Simon N. Lekakh

Missouri University of Science and Technology, Rolla, MO, USA

Abstract

Nonmetallic inclusions play a vital role for graphite nodule nucleation in cast iron with spheroidal graphite (SGI). Therefore, knowledge about composition of heterogeneous nuclei is practically important and can be used to control solidification in SGI castings. Thermodynamic simulations were performed to predict types of nonmetallic precipitates formed in the entire SGI processing, including melt nodularization and inoculation as well as followed melt cooling and casting solidification. To verify simulation results, the experimental SGI heats were performed with variations in nodularization and inoculation practices. Two types of specimens were collected. The first one was direct-quenched from the inoculated melt, and the second one was taken from the castings. An automated SEM/EDX inclusion analysis was used for evaluation of families of nonmetallic inclusions located in the matrix and inside graphite nodules. Nucleation activity of different precipitates was determined from the partitioning of active elements (Mg, Al, Si, Ca, Ce, La, Ti, Zr) between the graphite nuclei and the matrix. Simulation and experimental data were used to discuss a nucleation mechanism of graphite nodules in inoculated SGI. Engineering of nonmetallic inclusions can be used to control SGI solidification.

Keywords: *solidification, nucleation, cast iron, graphite nodules, nonmetallic inclusions*

Heterogeneous Nucleation of Graphite Nodules

Cast iron with spheroidal graphite (SGI) has a unique solidification structure with an unusually high volume density of solidification cells consisting of graphite nodules each surrounded by an austenite shell. A volumetric number of prime grains precipitated directly from the melt in SGI casting is larger than in other technical alloys solidified at a similar cooling rate (Figure 1). Mg-treatment blocks the growth of small graphite nodules in the Fe–C–Si melt, and this undercools melt and activates massive nucleation. This mechanism is not well understood. Qing et al.[1] studied the crystal structure of a graphite spheroid in the vicinity of its nucleus using high-resolution TEM. Crystal orientation maps of the graphite spheroid revealed misorientations and twist boundaries. High-resolution lattice fringe images showed that the basal planes of graphite were wavy and distorted close to the nucleus and very straight further away from it, while the mechanism behind this phenomenon is still unclear.

In an ideal case, the homogeneous liquid–solid transformation upon undercooling (ΔT) below the equilibrium solidification temperature (T_s) begins with randomly formed clusters. Clusters that are too small to survive are called embryos. This happens because an increase in Gibbs energy (ΔG_A) by the formed solid–liquid interface (A) is larger than the negative gain of Gibbs volume energy (ΔG_V):

$$\Delta G_A = A \Upsilon_{s-l} \qquad \text{Eqn. 1}$$
$$\Delta G_V = -V \rho L \Delta T / T_s \qquad \text{Eqn. 2}$$

where Υ_{s-l} is surface energy of the solid–liquid interface, V is volume, ρ is density, and L is latent heat per unit of mass. When the embryos are sufficiently large to be stable, they are termed nuclei. For spherical nuclei, a critical radius R_c at the homogeneous nucleation barrier is:

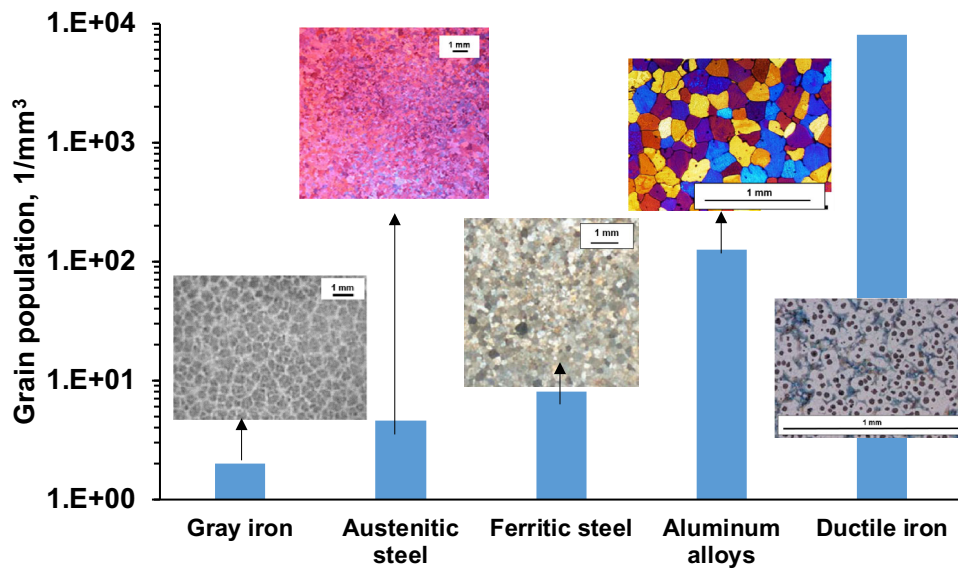$$R_c = 2 \Upsilon_{s-l} T_s / \rho L \Delta T \qquad \text{Eqn. 3}$$

Figure 1. Volumetric population of grains in solidification structure of different inoculated cast alloys.

$$\Delta T = 2\Gamma/R_c \qquad \text{Eqn. 4}$$

where $\Gamma = \Upsilon_{s\text{-}l}T_s/\rho L$ is the Gibbs–Thomson coefficient.

In the seminal article,[2] Turnbull evaluated $\Upsilon_{s\text{-}l}$ and Γ for several homogeneously nucleated metals from experimentally measured maximum supercooling achieved in small droplets. Recently, Hashimoto et al.[3] confirmed these predictions using molecular dynamic simulation of a solid–liquid interface. Homogeneous nucleation from stochastically formed nanometer scale embryos requires a deep undercooling of the metallic melt to overcome the energy barrier. Therefore, undercooling by a few degrees, which is typically observed in SGI, indicates heterogeneous nucleation on existing micron-sized particles. Because each graphite nodule forms independently, SGI solidification utilizes a large volumetric number of the active nucleation sites (10^3–10^4 per cubic millimeter). The ready active solid surfaces of nonmetallic inclusions in the melt will facilitate heterogeneous nucleation of graphite nodules by decreasing the total value of Gibbs energy in factor $f(\Theta)$:

$$\Delta G_{get} = \Delta G_{get}f(\Theta) \qquad \text{Eqn. 5}$$

where Θ is a contact angle on the triple junction between solid support, graphite nuclei and melt.

A typical SGI production process includes Mg-RE-Ca nodularization treatment to promote forming graphite spheroids and post-inoculation by a Fe–Si-based inoculant with active elements to facilitate heterogeneous nucleation of graphite nodules and decreasing the carbide forming tendency. The multiple possible reaction products can be formed during such complex SGI melt treatment. These precipitates could serve as the heterogeneous nucleation sites for graphite nodules. The reviews which summarized practical aspects of using Ce, La and the other RE metals for SGI were done by Skaland[4] and Riposan et al.[5] It was shown that a limited amount of RE improves SGI soundness, while extra Ce-additions could promote carbide forming. Liu[6] recently summarized the inoculation method of grain refinement of different alloys used in industry and provided an analysis of different related hypotheses. However, the factors that contribute to inoculation of graphite nodules are still not fully understood. Long et al.[7] found that La-sulfide acts as a heterogeneous site for graphite nucleation using contact-melting methodology. The estimated planar disregistries for graphite and *RE* compounds which were determined between (0001) graphite and (111) LaS, (0001) La$_2$O$_2$S, (111) YbS, (0001) La$_2$O$_3$, (111) *Yb$_2$O$_3$* and (0001) Yb$_2$O$_2$S and have values of 1.4%, 3.9%, 4.3%, 6.2%, 6.6% and 11.1%, respectively. A review of the actual heterogeneous nuclei compositions (oxides, sulfides and nitrides of Mg, Si, Ca, Ti, Ce, La) which were found inside graphite nodules was recently published by Alonso et al.[8] The observed graphite nucleation sites did not satisfy the principle of crystallographic similarity between solid support and graphite. It is possible that the atomic interactions between a solidified phase and a solid support are also important to facilitate heterogeneous nucleation. The authors[9] suggested evaluating the nucleation effectiveness of carbides and nitrides of transitional metals in iron alloys using the values of absorption energy of individual atoms on these phases. The ab initio simulations predicted bonding energy and could be used for the first selection of potential nucleation sites for graphite nodules.

Classical heterogeneous nucleation models assume that the melt above the liquidus temperature has ready potential nucleation sites. In this case, heterogeneous nucleation will

continue upon cooling below the liquidus temperature for a short initial period until the system reaches a maximal undercooling (ΔT_{max}). The major nucleation events will stop after that because all nucleation sites are used up and only few of them could stimulate the secondary nucleation wave at the end of solidification in the highly undercooled last portion of the liquid phase. However, Chisamera et al.[10] found that the Fe–Si inoculation with Ce, Ca, S, O additions provided bimodal nodule size distribution. It was observed that fewer large nodules formed at the start of solidification and a high number of much smaller nodules formed toward the end of solidification. Pederson et al.[11] and the authors[12–14] also described bimodal graphite nodule distributions in well-inoculated SGI. Recently, Yin et al.[15] directly observed two categories of graphite nodules using 3D X-ray micro-tomography, which were classified as precipitated in eutectic cell (large diameter) and located between cells (small diameter). These experimental observations indicate that heterogeneous nucleation of graphite nodules can continue during the entire solidification of SGI.

Thermodynamic Prediction of Nonmetallic Inclusion Family in Inoculated SGI

Multiple types of precipitates could be formed during SGI processing. Thermodynamic simulations based on the minimization of free energy of all chemical reactions in the melt (FactSage software[16]) are widely used for prediction of an equilibrium family of nonmetallic inclusions. Applied FToxid, FTOxCN and FStel databases include a variety of binary and complex stoichiometry phases and solid solutions. These simulations work well because chemical reactions between additions and elements dissolved in the iron proceed quickly and completed close to equilibrium in the high temperature. However, in addition to equilibrium precipitates, the multiple transient meta-stable precipitates could be also formed during inoculant dissolution and in the mushy zone during solidification. These transient meta-stable inclusions could play an important role in graphite nodule nucleation.[17]

In this article, formation of the thermodynamically stable and transient precipitates during an entire SGI process was analyzed using continuous simulations of the local equilibrium reactions. The formed transient inclusions could be dissolved back after melt equilibration. The tem meta-stable inclusions will be used in text. The equilibrium chemical reactions between active elements in nodulizer and dissolved elements in the melt were simulated. In addition, the chemical reactions in a supersaturated zone developed during dissolution of an Fe–Si-based inoculant and in a segregated mushy region of solidified SGI were also simulated (Figure 2). After each SGI melt treatment stage, the reaction products were "collected" assuming non-reversible reactions and the remaining

solution proceeded to cool and solidify with a step-by-step simulation of the local thermodynamic equilibrium. In these simulations, the melt with 3.6 wt%C, 2.5 wt%Si, 0.015 wt%S, 100 ppm $[O]$ and 50 ppm $[N]$ was treated by the Mg–Ce–La-type nodulizer and inoculated by Fe-75 wt%Si-based inoculant with active elements (Ca, Al).

Thermodynamic simulations showed that precipitates developed during SGI processing can be classified into three classes related to different conditions of their formation (Figure 2):

- *primary thermodynamically stable* precipitates developed in the melt during nodularization treatment with complex Mg–RE alloy;
- *primary meta-stable* precipitates formed during Fe–Si-based inoculant dissolution;
- *secondary thermodynamically stable and meta-stable precipitates* formed below the liquidus temperature in the mushy zone. Increasing affinity of [N],[S] and [C] to [Mg] and [RE] dissolved in the melt, and lowering temperature together with a positive segregation of these elements into the remaining melt, will promote the secondary precipitates formation during solidification. This category of precipitates includes nitrides, carbides and others compounds.

Figure 3 shows an example of simulated primary thermodynamically stable precipitates formed in the melt during treatment with Mg–Ce–La nodulizer at different ratios of RE metals and at constant 0.03% Mg addition. If only individual reactions will be considered, RE oxides will form by RE additions; however, when RE competes with the other active oxide former, such as Mg or Al, the formed products will depend on concentration of additions, initial levels of impurities and temperature. FactSage software simulates a minimum of free Gibbs energy considering the all possible reactions and indicates conditions when system will be equilibrated.

For these conditions, the reaction products contain one oxide (MgO) and multiple sulfides (MgS, Ce_2S_4 or La_2S_3). La has higher affinity to S than Ce and forms sulfide even at typically low (< 0.5) ratio of *La/Ce* in nodulizer. Figure 3a is plotted at constant 0.03 wt% Mg and 0.01% wt% Ce-additions. Decreasing temperature of SGI nodularization treatment increases affinity of all active elements to *S*, while it has a minor effect on oxide formation. Also, Mg-nitrides could be stable at a low temperature (Figure 3b). Such simulations can be performed to predict a particular family of precipitates during nodularization of industrial SGI with variation in impurities level (S, O, N) in the melt, nodulizer composition, element recovery and amount of additions. These reaction products are typically thermodynamically stable in the melt, but they could be floated
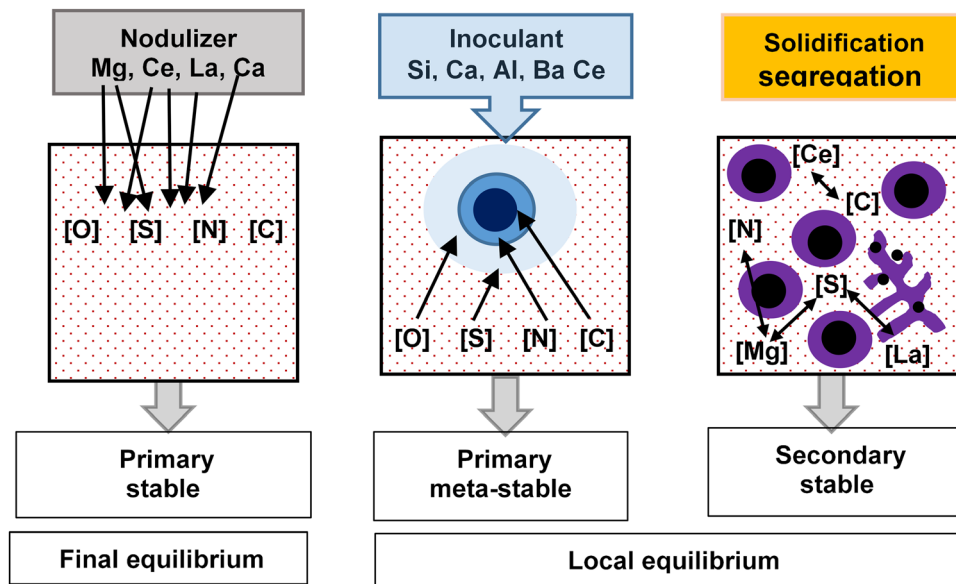
Figure 2. Simulation of reactions during SGI processing: (left) final equilibrium between dissolved in melt elements and active additions in nodulizer, (center) meta-stable precipitates in inoculant dissolution zones, and (right) segregation and reactions in mushy zone.
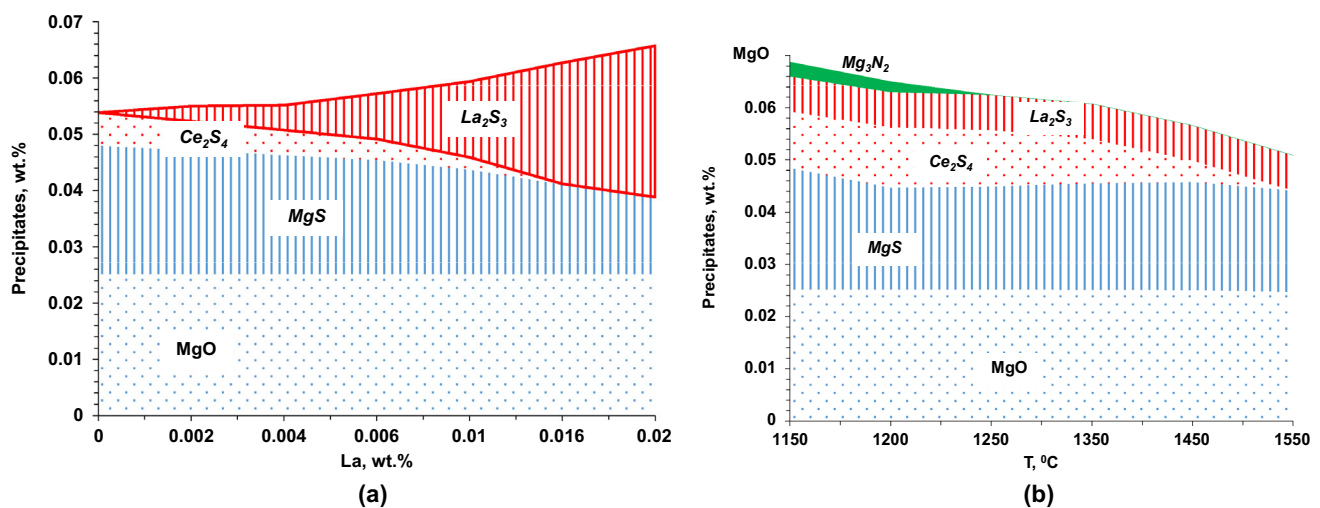

Figure 3. Simulated equilibrium reaction products in liquid SGI treated by Mg/Ce/La nodulizer: effect of La additions at 1550 °C (a) and temperature (b) at constant addition of 0.03 Mg, 0.01Ce and 0.005La into the melt with 3.6C, 2.5Si, 0.015S, 0.01O and 0.005 N (in wt%) assuming full recovery of additions.

out by different mechanisms (gravity Stokes flotation, melt convection, Ar-purge or filtration).

Equilibrium simulations showed that only few amount of new precipitates will be formed during Fe–Si inoculation of the Mg–RE treated melt, which cannot explain the effect of inoculation on increasing nodule count. Therefore, the local reactions in the melt during Fe–Si-based inoculant dissolutions needed to be calculated. Simulation of possible precipitates formed during 0.5 wt% inoculant addition (75 wt% Si, 1 wt% *Al*, 1 wt% Ca) was done by step-by-step

simulation of the dissolution zone in the melt. The formed reaction products were removed from the system after each simulation step. According to the simulations, the several precipitates can be formed during inoculant dissolution (Figure 4a). At initial stage of inoculant dissolution (low dissolution ratio), SiC and CaC_2 can be formed in the high silicon melt close to the surface of inoculant addition while it is dissolving, later AlN and some amount of MgS can also be precipitated. It is important to note that these reaction products have a meta-stable nature and can be re-dissolved back into the melt during holding.
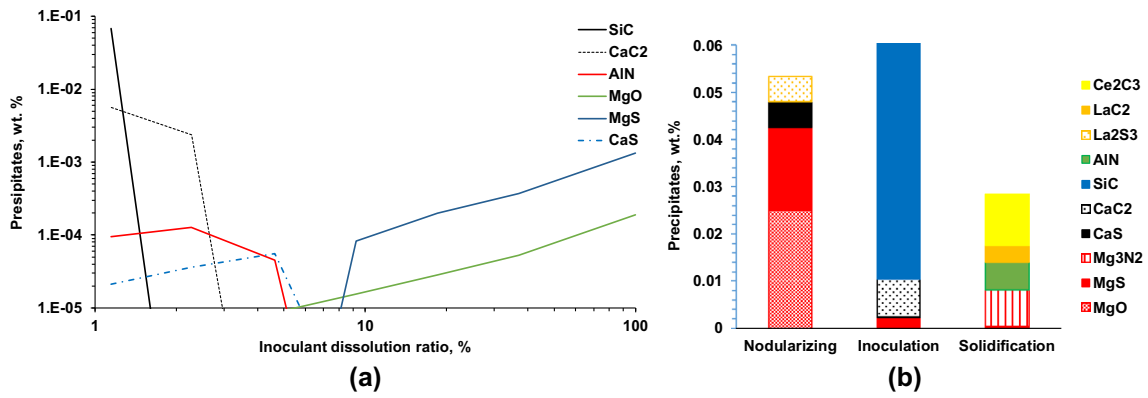
Figure 4. Simulated precipiates which could be formed during dissolution of 0.5 wt% inoculate (75 wt%Si, 1 wt%Al, 1%Ca) at 1400 °C (a) and families of all formed precipitates during entire SGI process (b).

Finally, a solid phase rejects the active elements into the melt during solidification. This segregation makes possible the precipitation of several thermodynamically stable and meta-stable secondary inclusions in the mushy zone. The family of these secondary inclusions contains Mg or Ti/Zr nitrides depending on the concentrations of these elements in the melt. It should be noted that extra amounts of RE metals, which were not involved in the formation of oxides and sulfides during previous process stages, could form undesirable carbides at the end of solidification. The amount of secondary precipitates increases during solidification, and they will be formed by the co-precipitation mechanism on the primary inclusions which are present in the melt. The families of all "extracted" precipitates during the entire SGI process simulation are shown in Figure 4b.

In addition, melt re-oxidation in the ladle and during mold poring could significantly change nonmetallic inclusion family. In particular, more stable oxides could be formed consuming active elements from nitrides. Figure 5

illustrates possible re-oxidation reaction products when oxygen was added into the treated SGI melt.

Experimental Searching Heterogeneous Nuclei in Graphite Nodules

The described thermodynamic simulations predicted a variety of formed precipitates during SGI processing, mold filling and casting solidification. However, the theoretical forecast of nucleation activity of these precipitates is not possible today. Therefore, an automated SEM/EDX analysis,[18] capable of investigating a large inclusion population, was adopted in this study to detect nuclei in graphite nodules. The used searching algorithm designated the inclusion center and collected EDX spectrum. This method provided an average chemistry in the case of complex inclusion. The effect of matrix for small inclusions was eliminated by applying the algorithms. Searching heterogeneous nuclei located on the middle of graphite nodules needs the large number of analyzed nodules because spheroidal graphite particle "shaded" nucleation core. A
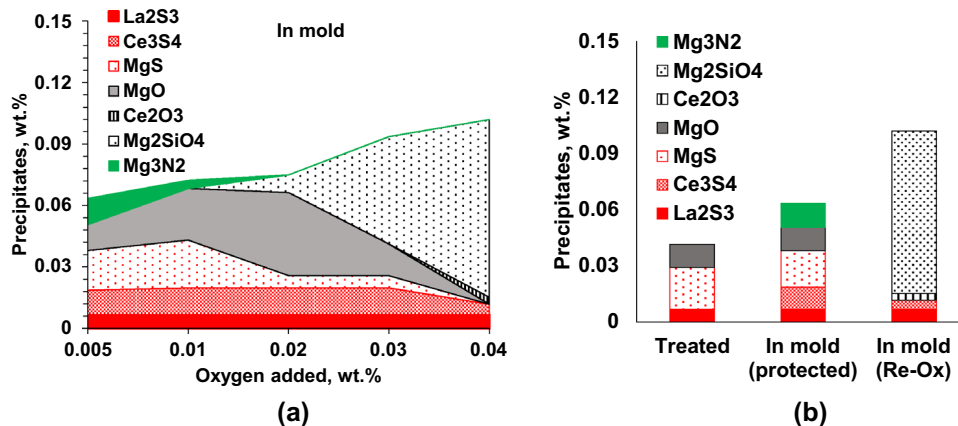

Figure 5. Simulated re-oxidation of treated SGI: (a) changing precipitate composition vs added oxygen and (b) possible change precipitate families during SGI processing without and with re-oxidation.
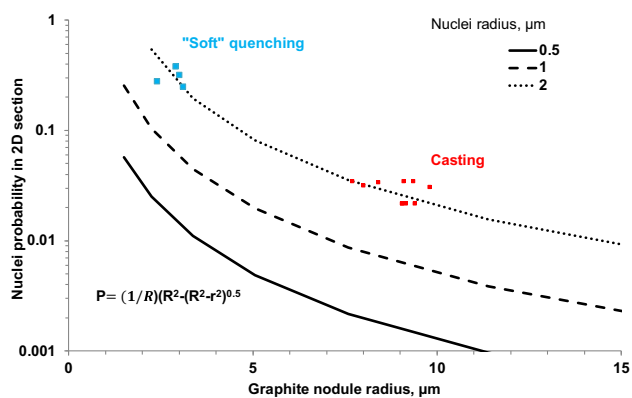
Figure 6. Calculated probability of detected nuclei in 2D polished section for different graphite nodule and nuclei radii. Dots illustrate experimental probability for cast and "soft quenched" specimens.

probability of "visible" nuclei in a random 2D section depends on a ratio of nuclei (r) and graphite nodule radii (R) (see the equation inserted in Figure 6). For typical few-micron-size nuclei, only several percent of analyzed nodules in a polished 2D section of casting will reveal the nucleation cores. To get the reasonable statistics, 8 000–10 000 nodules were searched in each sample which gave information about several hundreds of nuclei. To obtain the larger number, a "soft quenching" sampling method[19] was also used to develop 3–5 micron nodules in a specimen which significantly increased a probability of searching nucleation sites. The actual probabilities of searching nuclei inside graphite nodules for these two types of specimens are shown by dots in Figure 6. The experimental probability could be linked to an average nuclei diameter, but correction on depth of electron beam penetration is needed.

Experimental studies were performed using laboratory melted SGI from pure charge (0.004% S, 0.02% Cr, 0.03% Ni, 0.09% Cu, 0.01% Ti). Several heats were performed using two Mg–RE nodulizers (N1 with low RE (0.5%) and N2 with high RE (1.5%)) in combination with inoculant I1 (foundry grade Fe75Si) and inoculant I2 (2% Ce-bearing Fe75Si). Two sampling methods were used. The first "soft quenching" method provided a high cooling rate and small graphite nodules by direct sampling from the melt 4-mm thickness disk solidified between two steel plates (index "Q"). The second type of samples were taken from cast 15-mm plate solidified in no-bake mold, which provided slow cooling and larger nodules (index "Cast"). One industrial SGI produced from Ti-contaminated charge was also evaluated in addition to four clean laboratory produced SGI.

Two different settings of an automated SEM/EDX analysis were developed to detect and differentiate small non-metallic inclusions located in the metal matrix or inside

graphite nodules. Fine search with a small 0.5 micron step and high contrast was used to detect approximately 2000 inclusions in the matrix. A larger 2 micron step and low contrast was used for searching nuclei in 10 000 graphite nodules. Compositions of detected inclusions were plotted using joint ternary diagrams with three main elements on each.[18]
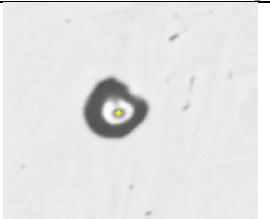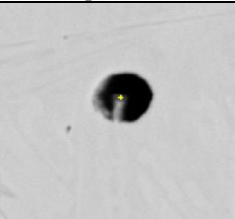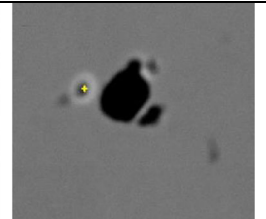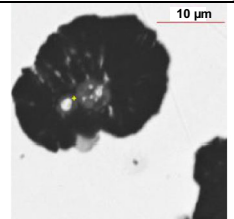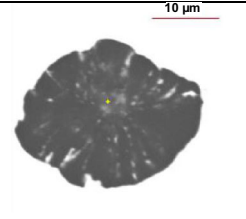
Examples of individual nonmetallic inclusions detected in the matrix and inside graphite nodules in quenched and cast specimens are shown in Table 1. A variety of inclusion morphologies were found inside graphite nodules. They include mono-phase inclusions formed in the melt and co-precipitated inclusions consisted of a primary core covered by a secondary shell formed during solidification.

Three classes of precipitates existing in the melt after inoculation were detected in the metal matrix of quenched specimen "Q": complex Mg–Al–Si nitrides, several complex Al–Si–Mg and Mg–Ce–La oxides and Mg–Ca and La–Ce sulfides (Figure 7). These types of reaction products in the melt were predicted by thermodynamic simulations (Figure 4b). A significant difference in nonmetallic inclusion families located in the metal matrix *vs* inside graphite nodules can be observed in ternary diagrams. Also, there is visible difference in nuclei family for quenched and cast specimens.

To quantify these differences, the average concentrations of active elements and their partitioning between inclusions sited inside graphite nodules ($E_{graphite}$, wt%) and the matrix (E_{matrix}, wt%) were calculated for all detected inclusions (Figure 8). *Ti* has a negative value of partitioning and sited mainly in the matrix, while Ca- and La-sulfides have tendency to form graphite nuclei. Graphite nuclei had significantly larger portion of La- and Ca-sulfides which indicated about it nucleation activity. The portion of sulfides detected inside graphite nodules decreased in the cast specimen when compared to rapid direct-quenched specimen. These changes in sulfide portion could be related to melt re-oxidation in the ladle and during mold pouring (Figure 5). The simulation results supported experimentally observed trends in re-oxidized melt (decreasing sulfides and increasing Mg–Si-oxides).

Four laboratory SGI with variations in melt additions were performed. Figure 9 presents observed changes in average inclusion compositions detected in the matrix and inside graphite nodules (possible nuclei) for combinations of different nodulizers and inoculants. Nuclei had significantly larger portion of La and Ca (mainly in sulfides) when compared to composition of inclusions located in the matrix for all practices. Application of high RE nodulizer N2 and inoculation with Ce-containing inoculant I2 increased amount of RE elements in nuclei and decreased Mg. The partitioning coefficients were significantly less than unit for Ti indicating about in-active role of Ti in

Table 1. Examples of Nonmetallic Inclusion Chemistries (wt%) Detected in Matrix and Inside Graphite Nodules in Quenched and Cast Specimens

Polished sections - quenched specimens		Polished sections of castings		
Nuclei *36La, 23Ce, 13S, 12O – core* *34La, 30Ce, 6Ca, 20S - shell*	**Nuclei** *Mg-Ca-S*	**In matrix** *45Ce, 23La, 13O, 7S*	**Nuclei** *Mg-Si-O*	**Nuclei** *Mg-Ca-S*

nucleation, while small total amount of Zr was mainly presented in nuclei chemistry. La- and Ca-sulfides were mainly detected in nuclei.

Cooling rate has visible effect on average graphite nodule nuclei chemistry in casting (Figure 10). Slow cooling in thicker casting plate increased the amount of elements involved in Mg–Si–Al nitride formation, while Ce-oxides and La-sulfides play important role in graphite nodule nucleation of the thin-walled SGI casting.

The effect of impurities in charge materials on detected graphite nuclei chemistry was verified using industrially produced SGI with 0.04% Ti. The specimens were taken from 18-mm keel block poured into a green sand mold. Ternary diagrams of inclusions found indicated about a large amount of *TiN* in the matrix (Figure 11a); however, significantly less Ti was found in nuclei (Figure 11b). In this SGI, Ti and Zr have partitioning coefficient less than unit. Ca- and La-sulfides and Ce-oxides were mainly detected in nuclei.

Discussion: Principles of Engineering of Nonmetallic Inclusions to Control Graphite Nodule Nucleation

Engineering Inclusion to Control Solidification

Thermodynamic simulations and an experimental searching methodology of graphite nodule nuclei can be used for optimization of SGI processing. The term *engineering of nonmetallic inclusions in SGI for controlling graphite nodule nucleation* is suggested to describe this methodology. Engineering of nonmetallic inclusions to control graphite nodule nucleation could be considered as one of the more broad methods of liquid metal engineering (LME) which refers to a variety of physical and/or chemical

treatments of the molten metals aimed at influencing their solidification characteristics.[20] In particular, the SGI melt treatment optimization could done by development of:

– *types of nonmetallic inclusions* to initiate heterogeneous nucleation of graphite nodules;
– *sequence of precipitate formation* for prolongation of nucleation events until the end of solidification;
– *topology* of these precipitates (dimension, number and shape) to be active nuclei.

The types of nonmetallic inclusions and sequence of their formations were determined in this study by using thermodynamic simulations and an automated SEM/EDX analysis. The nucleation activity could be defined experimentally based on partitioning coefficient of the active elements.

A classical approach of solidification analysis assumes instantaneous heterogeneous nucleation of graphite nodules at maximal undercooling on the ready random distributed primary heterogeneous nucleation sites in the melt. Theoretically, this mode will provide a near lognormal distribution of 3D diameters of cast grains. However, the experimental data[10–13] indicate a more complex graphite nodule distribution in inoculated SGI castings which could be related to continuous nucleation toward the end of solidification and a possible second nucleation wave. Figure 12 illustrates 3D population density function (*PDF*) of graphite nodules. *PDF* was calculated as the frequency of graphite nodules in a given size bin, and the shape of PDF does not depend on bin size. The method of conversion of SEM/EDX measured 2D nodule diameters to 3D conversion was described in publication.[14] Theoretically, the structure of instantaneously nucleated alloy can be presented by straight line in *ln(PDF)-ln(D)* coordinates. However, the graphite nodule distribution curves in studied SGI were parabolic. Moreover, SGI treated with RE
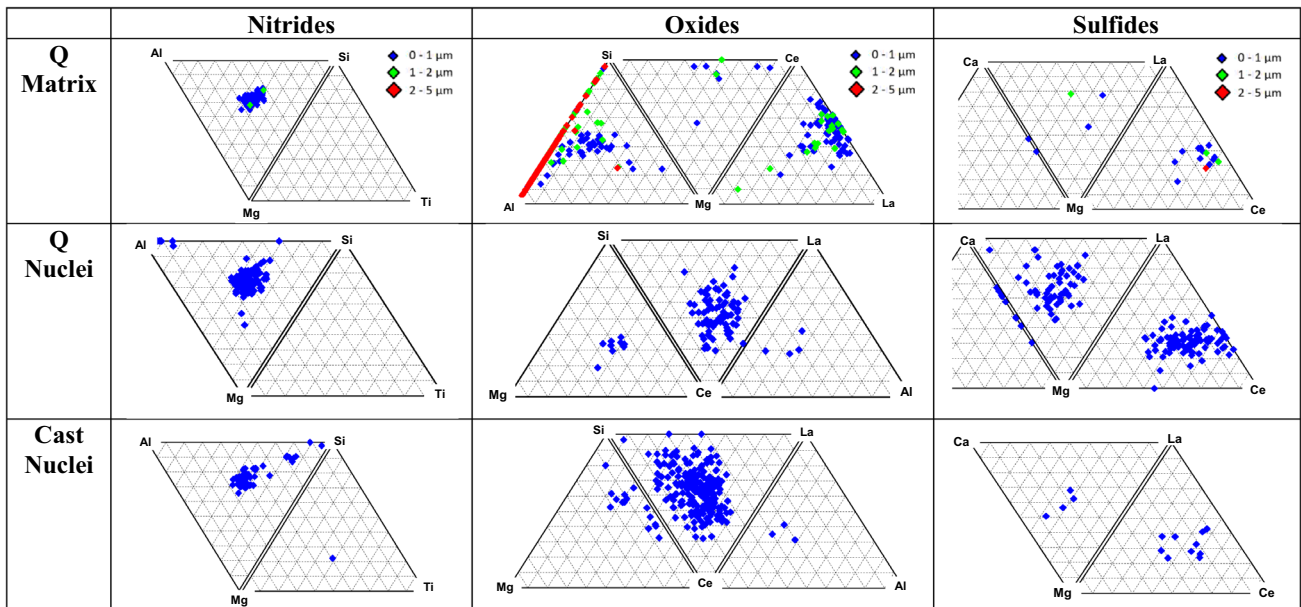
Figure 7. *Ternary plots of nonmetallic inclusion families (nitrides, oxides and sulfides) detected in matrix and inside graphite nodules in quenched (Q) and cast specimens (SGI treated by nodulizer N1 and inoculated by I2).*
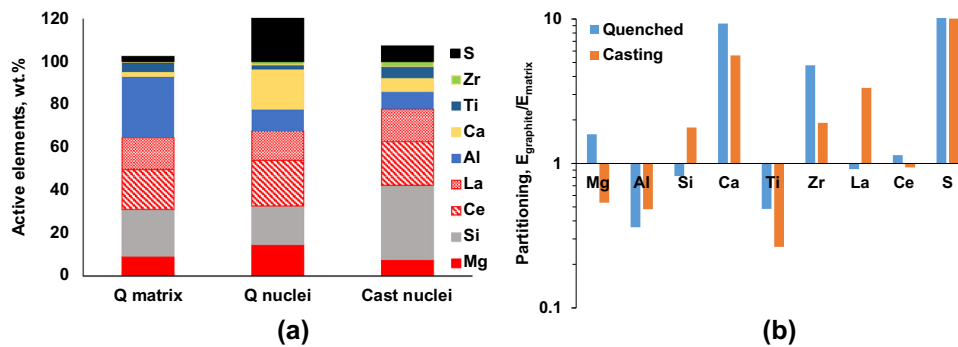

Figure 8. *Average composition of active elements (S plotted above 100%) (a) and partitioning coefficients of active elements between nuclei and matrix in SGI (N1, I2).*
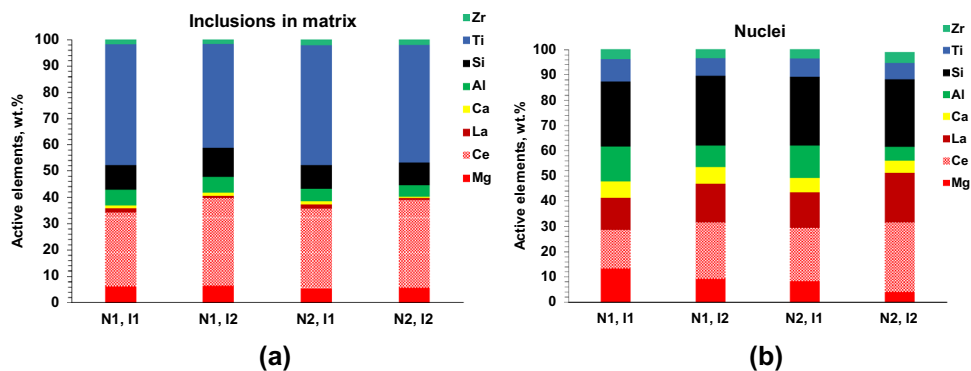

Figure 9. *Effect of nodulizer and inoculant compositions on average concentration of active elements in nonmetallic inclusions located in the matrix (a) and found inside graphite nodules (b).*

additions (N2, I2) provided bimodal distribution of graphite nodules which can be linked to the second nucleation wave toward the end of solidification.

To prove evidence of continuous nucleation, high-resolution μCT scan was performed on Ce-inoculated N2, I2 SGI by the authors.[21] There are several possible space
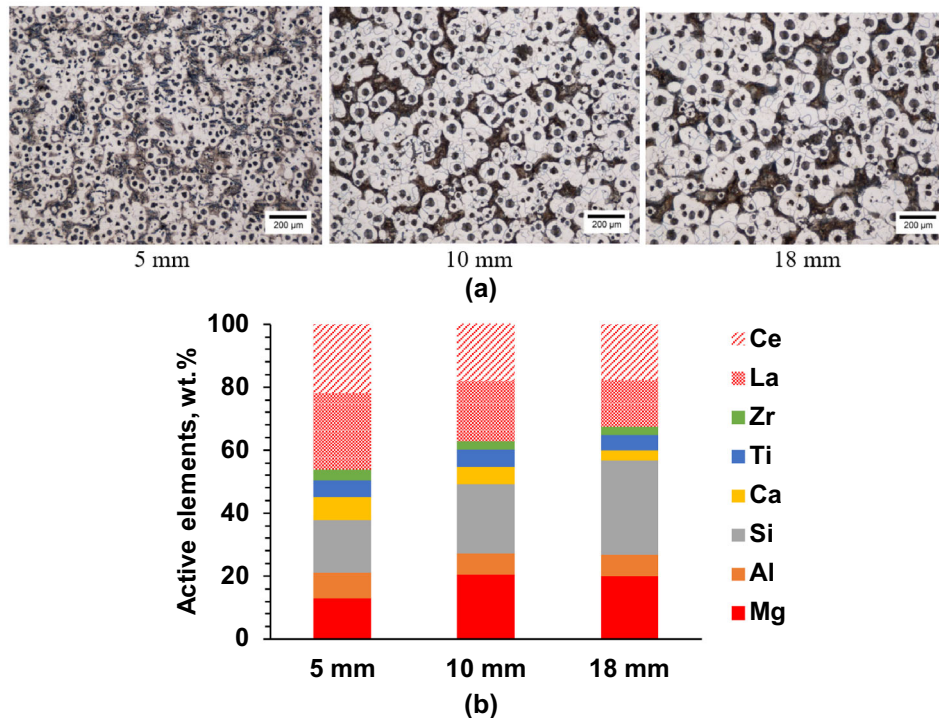
Figure 10. Effect of cooling rate (wall thickness) on structure (a) and nuclei composition in laboratory melt SGI (b).

distribution fabrics of graphite nodules: (i) near random distribution in the case of instantaneous nucleation or (ii) clustered and their combinations in the cases of continuous nucleation or several nucleation waives. To verify a 3D space distribution fabric in SGI, all graphite nodules in structure were divided into three equal classes by nodule number: small, medium and large (Figure 13a). Color code was applied: blue for large, green for medium and red for small nodules. To better visualize space distribution fabric, Figure 13b and c illustrates trimmed volume with graphite nodules from each group. Clustered groups consisting of 5–10 small nodules were located in a specific space which could represent interdendritic regions where the cast iron solidified at the end. This means that a family of heterogeneous nuclei changed during solidification and new or secondary active nucleation sites were developed during the solidification process. Continuous nucleation promotes small nodules in the final cast structure.

Topology of Secondary Precipitates and Heterogeneous Nucleation Activity

Ready active solid surfaces of nonmetallic inclusions in the SGI melt facilitate the heterogeneous nucleation of graphite nodules by decreasing the total value of Gibbs energy by a factor $f(\Theta)$ (Eq. 5). The analytical equation $f(\Theta)$ was proved for the case when nuclei cap contacts with an infinitely flat supporting surface. However, the value of this factor depends not only on the contact angle Θ but also on the 3D geometry of a supporting surface.[22] To verify the

real 3D geometry of nonmetallic inclusions formed in a laboratory-produced SGI, its electrolytic extraction was performed.[14] Table 2 illustrates extracted phases from quenched and cast specimens. It can be seen that co-precipitated nitrides on oxide and sulfides cores form a complicated convex/concave faceted shape with 90° internal corners.

The ternary diagrams of 3D extracted nitrides, sulfides and oxides (Table 3) were similar to diagrams for 2D sections of inclusions found in the matrix (Figure 6); however, extracted 3D inclusions were large sizes.

Because the nonmetallic inclusions formed in SGI have a complicated surface topology, SE-FIT software[23,24] was used to simulate an equilibrium shape of nuclei with a minimal surface energy. A nucleus was simulated as a droplet sited on different geometry surfaces for a particular contact angle. The simulated shape of a liquid droplet on an infinite substrate depended on contact angle, and simulated $f(\Theta)$ was in agreement with Eq. 5. Decreasing the contact angle on an infinitely large substrate reduced the relative undercooling for heterogeneous nucleation. However, the effect of the contact angle on undercooling depends on a support dimension L. When a nucleus with radius R sits on a small substrate and contact its boundary, decreasing the contact angle does not reduce a critical undercooling (Figure 14a). Therefore, a larger than a minimal K-ratio ($K = L/R$) is needed to facilitate heterogeneous nucleation.
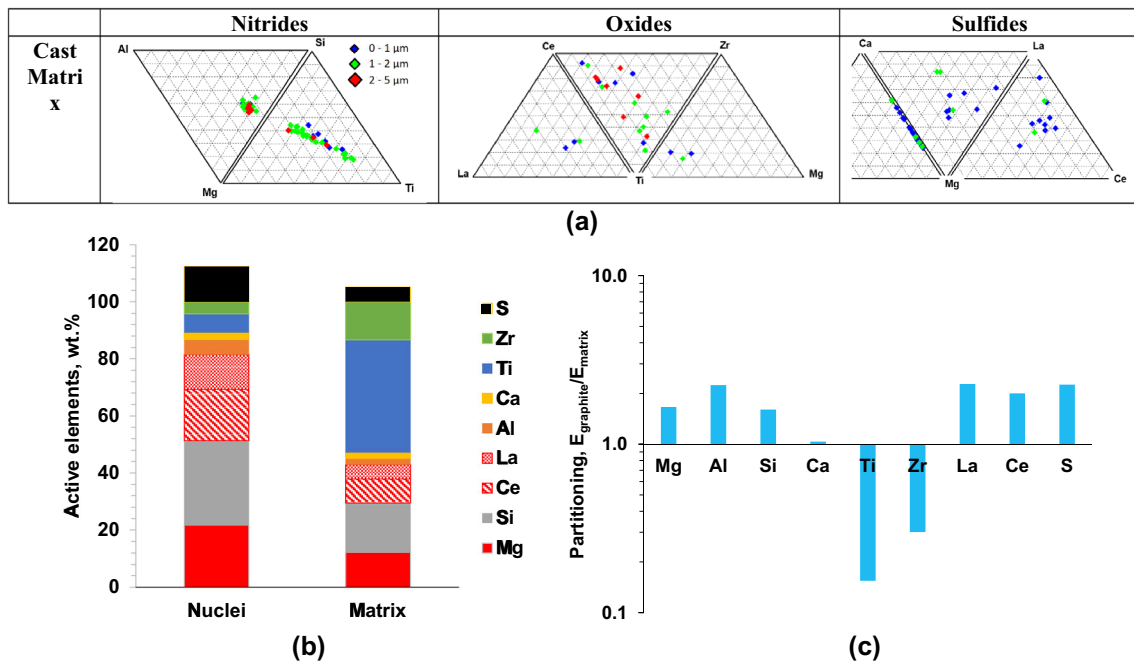
Figure 11. Classes of nonmetallic inclusions in industrial SGI contaminated by 0.04% Ti: (a) ternary diagrams for nitrides, oxides and sulfides located in the matrix, (b) average compositions of inclusions located inside graphite and in matrix and (c) element partitioning in inclusions found in graphite and matrix.
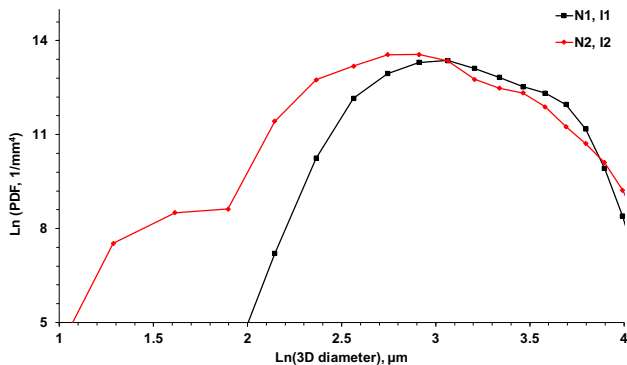

Figure 12. Population density function (PDF) of graphite nodules in Ln(3D)/Ln(PDF) coordinates for two SGI practices.

The second factor is related to the geometry of the potential nucleation site. The secondary co-precipitated inclusions can be formed during cooling and in the mushy zone on the primary inclusion presented in the melt. Co-precipitation mechanism typically develops a complicated surface topology. An example of the 3D shape of electrolytically extracted inclusions is shown in Table 2. A more detailed TEM electron diffraction study[25] revealed a crystallography of later formed nitrides precipitated on an existing oxide particle in a grain refined iron alloy. Co-precipitated nitrides had a combination of joint concave and convex atomically flat folded faceted surfaces. SE-FIT simulation showed that the folded inclusions with angle $\beta < 2\pi$ have a significant nucleation advantage relative to a flat support (Figure 14b). Therefore, folded secondary inclusions, formed by a co-precipitation mechanism, will generate the additional sides for continuous nucleation.

Conclusions

Thermodynamic simulations were used to predict non-metallic inclusion family formed in the melt during nodularization and inoculation treatment as well as in solidified SGI solidification. An automated SEM/EDX analysis was used for searching the graphite nodule nuclei in pure laboratory-produced and *Ti*-contaminated industrial SGI. The method for determination of nucleation activity of different precipitates[24,26] was discussed. This method is based on analysis of distribution of active elements between inclusions being nucleation sites inside graphite nodules and located in the metal matrix. It was shown that Ca- and La-sulfides, Ce-oxides and Mg–Al–Si nitrides concentrated mostly inside graphite nodules. Melt treatment, impurities and cooling rate changed the chemistry of inclusions found inside graphite nodules. The principles of engineering of nonmetallic inclusions to control graphite nodule nucleation and casting solidifications were discussed.
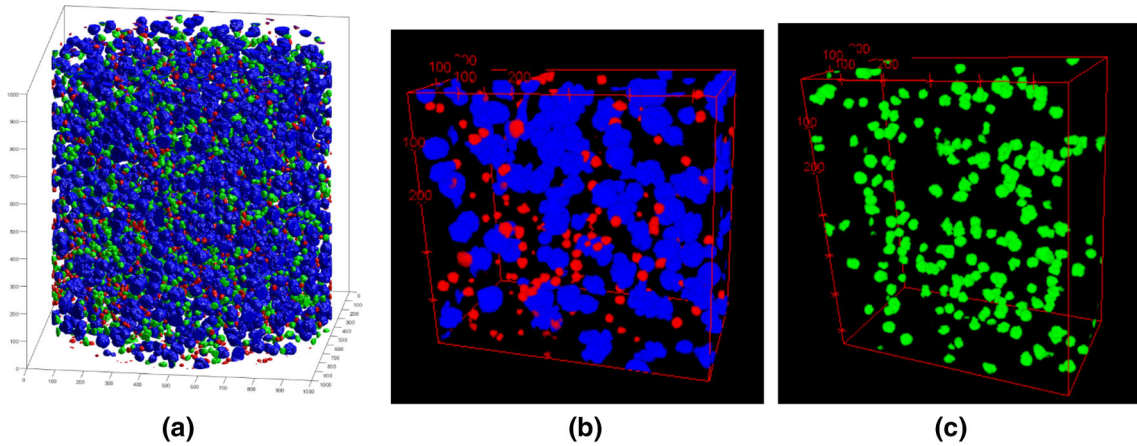
Figure 13. μCT scan of N2, I2 SGI: (a) with color code for large (blue) > 25 μm, medium (green) 16–24 μm and small (red) < 16 μm nodules, (b) trimmed volume with groups of small graphite nodules (red) clustered between ordered large nodules (blue) and (c) clustered medium diameter nodules (green).[21]

Table 2. 3D Shape and Chemistry (wt%) of Electrolytically Extracted Phases from the Matrix of SGI Casting

Extracted from quenched specimens			Extracted from castings		
Graphite	**Oxi-sulfide** 30*Ce*, 29*La*, *17*S, *11*O	**Complex Oxide** 25*Ca*, 10*Mg*, 60*O*	**Co-precipitated** 29*Ce*, 9*Ca*, 19*S* – white 26*Si*, 14*Al*, 13*Mg*, 12*O* - gray	**Faceted** 9*Mg*, 8*Si*, 6*Al*, 70*N*	**Co-precipitated** 10*Mg*, 63*O* - top *SiC* - bottom

Table 3. Ternary Diagrams of Nitrides, Oxides and Sulfides Extracted from Casting Matrix (N2, I1)

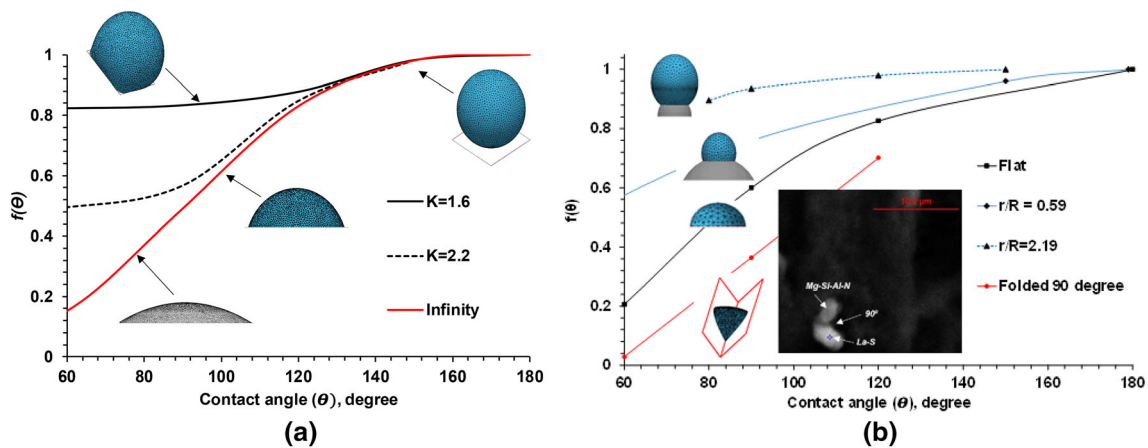|	Nitrides	Oxides	Sulfides
Extracted Cast Matrix			
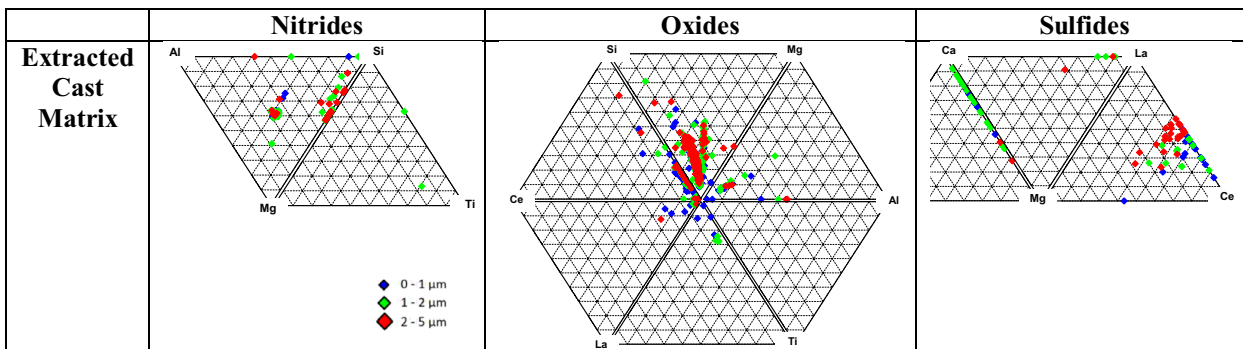
Figure 14. *Joint effects of contact angle (θ) and dimensional ratio K (a) and shape of nuclei (b) on function f(θ) (SE-FIT/Surface Evolver software).*[24]

REFERENCES

1. J. Qing, V. Richards, D. Van Aken, Carbon **5**, 456 (2017)
2. D. Turnbull, J. Appl. Phys. **21**, 1022 (1950)
3. R. Hashimoto, Y. Shibuta, T. Suzuki, ISIJ Int. **51**(10), 1664 (2011)
4. T. Skaland, in Keith Millis Symposium on Ductile Cast Iron 2003
5. I. Riposan, M. Chisamera, V. Uta, S. Stan, R. Naro, D. Williams, in Keith Millis Symposium on Ductile Cast Iron 2003
6. Z. Liu, Metal. Mater. Trans. A **48A**, 4755 (2017)
7. K. Long, H. Sasaki, H. Kimura, T. Yoshikawa, M. Maeda, ISIJ Int. **58**(1), 123 (2018)
8. G. Alonso, D. M. Stefanescu, R. Larranaga, R. Suarez, E. De la Fuente, in *AFS Proceedings*, Paper 17-031 2017
9. S. Lekakh, N. Medvedeva, Comp. Mater. Sci **106**, 149 (2015)
10. M. Chisamera, I. Riposan, S. Stan, M. Barstow, in *AFS Proceedings*, Paper 12-071 2012
11. K.M. Pedersen, N.S. Tiedjie, Mater. Charact. **59**, 1111 (2008)
12. S. Lekakh, ISIJ Int. **56**(5), 812 (2016)
13. S. Lekakh, B. Hrebec, Int J Metalcasting **10**(4), 389 (2016)
14. S. Lekakh, in *AFS Proceedings of the 122nd Metalcating Congress,* 2018, Fort Worth, TX, Paper 18-083
15. Y. Yin, Z. Tu, J. Zhou, D. Zhang, M. Wang, Z. Guo, C. Liu, X. Chen, Met Mat Trans A **48**(8), 3794 (2017)
16. Factsage software, www.factsage.com
17. N. Muhmond, H. Fredriksson, Met Mater Trans, B **44B**(2), 283 (2013)
18. M. Harris, O. Adaba, S. Lekakh, R. O'Malley, V. Richards, in A*ISTech Proceedings* 2015 p. 3315
19. S. Lekakh, V. Richards, K. Peaslee, Int J Metalcasting **4**, 25 (2009)
20. F. Czerwinski, Met Mater Trans, B **48B**, 367 (2017)
21. S. Lekakhl, X. Zhang, W. Tucker, H.K. Lee, T. Selly, J. Schiffbauer, micro-ct quantitative evaluation of graphite nodules in sgi. Int J Metalcasting (2019). https://doi.org/10.1007/s40962-019-00354-9. **(in press)**
22. T.E. Quested, A.L. Greer, Acta Mater. **53**, 2683 (2005)
23. SE-FIT Software, Portland State University, www.se-fit.com. Accessed May 2018
24. S. Lekakh, Met Mater Trans, B, v **50B**, 890 (2019)
25. S. Lekakh, J. Ge, V. Richards, R. O'Malley, J. Terbush, Met Mater Trans B **48B**, 406 (2017)
26. S. Lekakh, Int. J Metalcasting,v **13**(1), 47 (2019)